The International Journal of Advanced Manufacturing Technology (2024) 130:5869–5878
https://doi.org/10.1007/s00170-024-13120-x

ORIGINAL ARTICLE

Energy efficiency improvement method of magnetic pulse welding based on auxiliary capacitance

Wentao Liu[1] · Wenxiong Peng[1] · Zhi Li[1] · Huaiqing Zhang[1]

Received: 20 May 2023 / Accepted: 22 January 2024 / Published online: 27 January 2024

Abstract

To solve the problem of energy loss caused by low energy utilization rate in the process of magnetic pulse welding (MPW), this paper presents a method to recover the energy after the first half wave of pulse current by using auxiliary capacitance. A detailed introduction of the working process of the improved discharge circuit was first carried out. Then experimental investigation of the current waveform of the main discharge circuit and analyzed numerically of the improved MPW system were investigated. The experimental results of the current waveform of the main discharge loop agree well with the simulation results, which verifies the feasibility of the proposed method. The simulation results show that the energy loss decreases from 95.3% before the improvement to 36% after the improvement, and the energy utilization rate increases by 261.5%. According to the welding window theory, the welding quality of this method is the same as that of the traditional method. It shows that this method can greatly improve the energy utilization rate of magnetic pulse welding without reducing the welding quality and verifies the effectiveness of this method.

Keywords Energy recovery · Auxiliary circuit · Electromagnetic pulse welding · Welding window

1 Introduction

In the field of manufacturing, to meet the new development requirements of lightweight, low-cost, and structural function integration of industrial design, single structural materials are gradually changing to composite structural materials. Welding is a common means to change a variety of single materials into composite materials, but the traditional fusion welding technology has obvious defects, such as different materials having different thermal properties, which will lead to fusion welding defects [1, 2]. In addition, some specific alloys are sensitive to heat, for example, aluminum 7075 alloy is easy to crack at high temperature [3, 4]. Titanium has strong chemical activity at high temperatures [5, 6].Therefore, as a solid welding technology, magnetic pulse welding has attracted much attention in recent years. In solid welding, defects such as cracking, deformation and porosity caused by the liquid phase in fusion welding can be avoided [7]. With the deepening of the research, scholars found that the magnetic pulse welding process has the advantages of environmental friendliness, low welding temperature, fast welding speed, and high-quality welding parts [8].

In the process of magnetic pulse welding, the pulse current presents a sinusoidal oscillation attenuation trend, and the time interval of flyer plate movement in the welding process is in the first positive half of the current [9]. The welding ended after the first positive half of the current. This causes a large amount of energy waste, and the energy utilization rate is less than 5% [10]. This shortcoming limits the research, development and application of MPW, so how to improve the system's energy efficiency becomes an important issue in the development of MPW technology. Khalil et al. designed an O-coil structure to improve coil efficiency. Compared with the I-coil, the peak current and current frequency increase by 10%, and the simulation results show that the impact velocity of the plate is higher [11]. Zhang et al. analyzed the optimization of the structural parameters of the E-coil in MPW and proposed a set of coil structural parameters to improve the magnetic pressure on the surface of the flyer plate and thus improve the energy utilization rate [12]. Deng et al. optimized magnetic pulse spot welding with the help of a field shaper. Numerical analysis showed that

✉ Wenxiong Peng
pwx@cqu.edu.cn

[1] State Key Laboratory of Power Transmission Equipment & System Security and New Technology, Chongqing University, Chongqing 400044, People's Republic of China

with the increase of the aperture, the impact velocity of the plate first increased and then decreased, and the system efficiency could be improved by modulating the aperture [13]. Li et al. designed and developed a modularized MPW system with adjustable frequency. This study found that when the discharge energy remained constant, the peak current and the deformation velocity of the fly plate were proportional to the discharge frequency, so increasing the discharge frequency could effectively improve the welding effect and the energy utilization rate of the system [14]. Li et al. analyzed the circuit parameters of the system and found that reducing the circuit inductance could improve the system efficiency, and proposed a scheme to replace the circular transmission cable with copper bar to reduce the total inductance of the circuit [10]. Li et al. designed a multi-weld coil to increase the welding area of a single weld and thus improve energy utilization [15].

In the above research, the main means to enhance the energy efficiency of the MPW system is to optimize the design of coil, field shaper, and circuit parameters. Although these methods can improve the system, there is still a lot of wasted energy, so the effect of improving the system's efficiency is not significant. Therefore, an energy recovery scheme based on bypass capacitance is proposed in this paper, and the scheme is introduced.

2 MPW system

The equivalent circuit of the MPW system consists of two circuits: a charging circuit and a discharge circuit. The charging circuit is composed of a charging power supply and a capacitor bank. Its function is to provide the initial voltage to the discharging capacitor, that is, to provide energy. The discharge circuit consists of a capacitor bank and a drive coil, as shown in Fig. 1a. When the discharge loop is connected, the electric energy stored in the capacitor is released into the drive coil as a pulse current, generating a strong pulsed magnetic field B around it. According to Lenz's law, the flyer plate and the drive coil will generate a huge repulsing electromagnetic force, and the flyer plate will quickly collide with the base plate under the driving force, as shown in Fig. 1b.

When the relative velocity and collision angle of the two plates are appropriate, metallurgical bonding will be formed [16]. The electromagnetic force can be expressed as follows:

$$F = J \times B \tag{1}$$

When the flyer plate is displaced, the mutual inductance between the drive coil and the flyer plate will be affected, so the theoretical calculation of discharge current is very

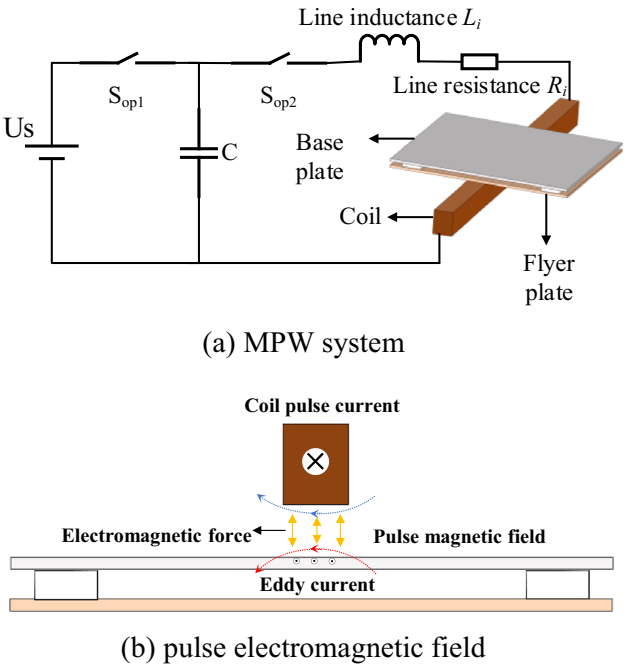

Fig. 1 MPW system diagram and pulse electromagnetic field diagram

complicated. However, as the duration of the whole welding process is very short, the influence of this part can be ignored, and the discharge circuit can be equivalent to an RLC circuit, as shown in Fig. 2.

In Fig. 2, R is the total resistance of the circuit, including line resistance, coil resistance and internal resistance of switches and capacitors. L is the total inductance of the circuit, including line inductance, coil inductance, switching inductance, and capacitor stray inductance. C is the capacitance of the capacitor bank. Therefore, the discharge circuit equation is as follows:

$$RI + L\frac{dI}{dt} + \frac{1}{C}\int Idt = 0 \tag{2}$$

In this equation, resistance, inductance, and capacitance must satisfy the following:

$$R < 2\sqrt{\frac{L}{C}} \tag{3}$$

At this time, the coil current is as follows:

$$I(t) = \frac{U_0}{\omega_d L} e^{-\alpha t} sin\omega_d t \tag{4}$$

where ω_d is the equivalent angular frequency and α is the attenuation coefficient.

A typical discharge current waveform is shown in Fig. 3.

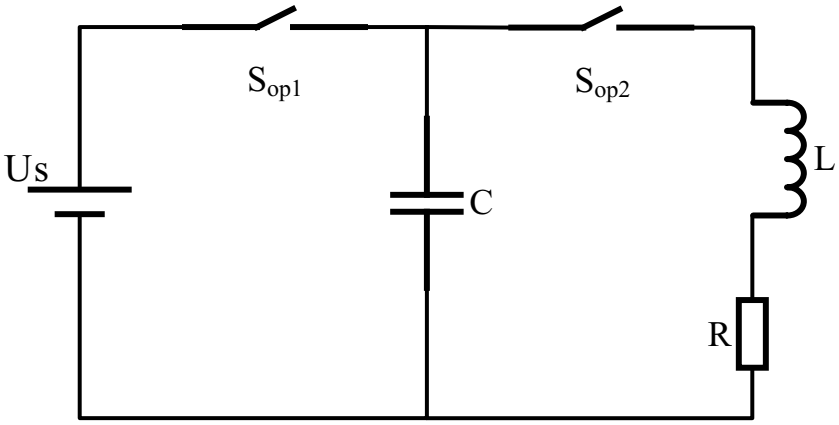

Fig. 2 Equivalent circuit of the discharge circuit

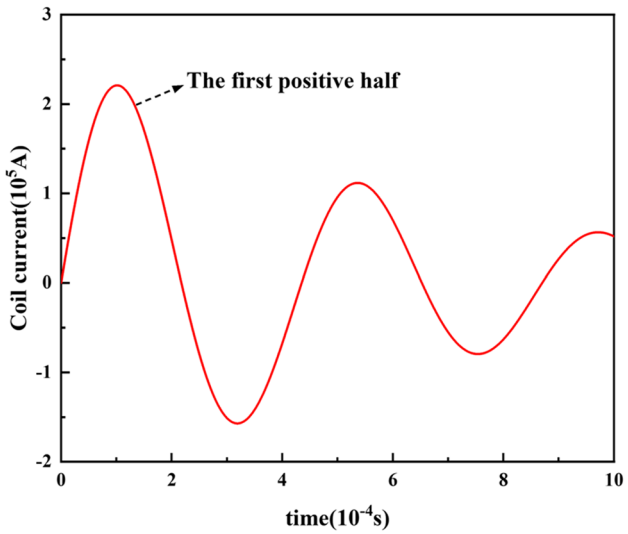

Fig. 3 Typical discharge current waveform

3 The improved MPW circuit

In the previous section, the pulse current equation and waveform of conventional MPW were introduced. When the current is in the first positive half cycle, the capacitor voltage has entered the negative half cycle. According to this characteristic, a high-power diode (D_1) and a pulse capacitor (C_2) are added at both ends of the capacitor. When the voltage of the discharge capacitor enters the negative half cycle, the D_1 enters the on state. To maximize the energy utilization rate, a high-power diode (D_2) is also connected in series on the main discharge circuit. When the main discharge current enters the negative half cycle, the D_2 enters the off state. The improved MPW circuit is shown in Fig. 4.

In the initial stage of discharge, the improved circuit and the original circuit working principle are the same, closing Sop_1, making the discharge circuit conduction, generating pulse current on the drive coil, so that the fly plate under the drive coil induction pulse current, fly plate current and drive coil current opposite, so that between the fly plate and the drive coil produces a great electromagnetic repulsive force, which

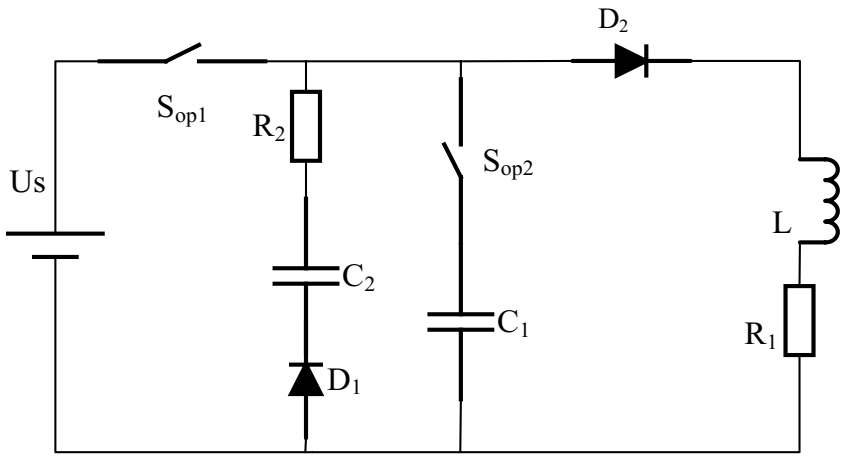

Fig. 4 Improved MPW circuit

driving flyer plate deforms at high speed and collides with the base plate. This stage is hereinafter referred to as the first discharge stage. The difference is that when the voltage of the discharge capacitor is reversed, the bypass capacitor branch enters the on–off state, and the on–off of the branch will affect the current waveform of the main discharge circuit. This stage is hereinafter referred to as the second hotel stage. When the main circuit current decays to zero, the discharge capacitor will only discharge the bypass capacitor branch until the voltage of C_1 is equal to that of C_2. This phase lasts very short. This stage is hereinafter referred to as the third discharge stage.

The working process of the improved MPW circuit is divided into four stages, as shown in Fig. 5.

In charging stage, circuit breaker Sop_1 is closed, and the primary power supply charges the capacitor C_1 until the voltage of the capacitor C_1 equals the voltage of the primary power supply to U_0.

In the first discharge stage, after the end of charging, Sop_1 is turned off; Sop_2 is closed; the main discharge circuit is connected; and the capacitor C_1 begins to discharge. The circuit voltage equation and the instantaneous expression of the circuit current in this discharge stage are as follows:

$$U_{C1}(t)_{t=0^+} = U_0 \tag{5}$$

$$RI + L\frac{dI(t)}{dt} + \frac{1}{C}\int Idt - U_0 = 0 \tag{6}$$

$$I(t) = \frac{U_0}{\omega_d L}e^{-\alpha t}sin\omega_d t \tag{7}$$

In the second discharge stage, because the load is resistance-inductance load, the loop current lags behind the voltage of capacitor C_1, that is, when capacitor C_1 ends the first positive half cycle, the main discharge circuit is still in the first positive half cycle. At this time, the voltage of capacitor C_1 will increase in the reverse direction, and the high-power diode of the bypass capacitor branch will be in the state of positive voltage. The tube will be switched on, and capacitor C_1 will then charge capacitor C_2. The circuit voltage equation and node equation of the circuit at this stage are as follows:

$$R_1 I_L(t) + L\frac{dI_L(t)}{dt} - \frac{1}{C_1}\int I_{c_1}dt = 0 \tag{8}$$

$$\frac{1}{C_1}\int I_{c_1}dt + \frac{1}{C_2}\int I_{c_2}dt + I_{c_1}(t)R_2 = 0 \tag{9}$$

$$I_{c_2}(\mathrm{t}) - I_L(\mathrm{t}) = I_{c_1}(\mathrm{t}) \tag{10}$$

In the third discharge stage, when the current of the main discharge circuit decays to zero, the diode of the main discharge circuit will be turned off, that is, the main discharge circuit is disconnected. At this time, only *C*1 and C_2 circuits remain. Because the C_1 voltage is higher than the C_2 voltage at the moment the main discharge circuit is disconnected, C_1 will continue to discharge to C_2. The

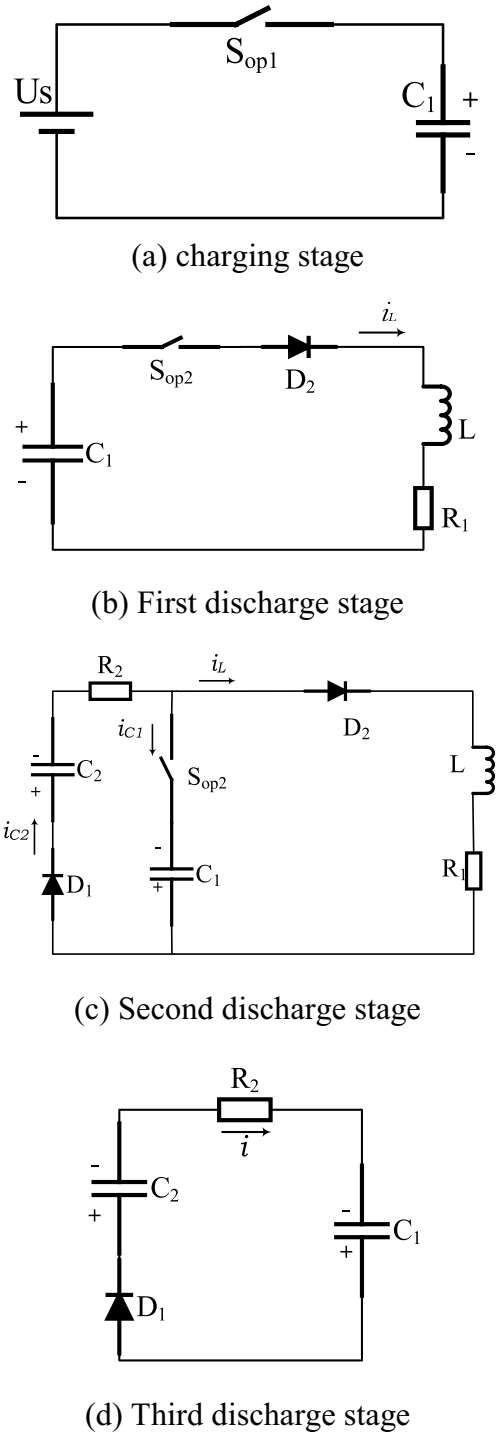

Fig. 5 Working process of improved MPW circuit

circuit voltage equation at this stage can still be expressed by Eq. (9), and the current equation becomes

$$-I_{c_1}(t) = I_{c_2}(t) \tag{11}$$

That is

$$-C_1 \frac{dU_{C_1}(t)}{dt} = C_2 \frac{dU_{C_1}(t)}{dt} \tag{12}$$

To make the energy utilization rate more clear, the energy provided by the primary power supply to discharge capacitor C_1 at the charging stage is defined as the total energy storage E_{sys} of the system. In the first and second discharge stages, the energy used to provide the flyer plate welding and the energy lost in the discharge process is E_{sec}, that is, the energy consumed by the system during a single welding process. At the end of welding, the energy stored in capacitors C_1 and C_2 is E_{rec}, which is the total energy recovered by the system. In the process of single welding, the effective work done by the system should be E_{k} done to the flyer plate by the electromagnetic force between the driving coil and the flyer plate during the discharge process. During single welding, the system energy loss is E_{loss}. Before improvement, the energy efficiency of the system can be expressed as follows:

$$\eta_1 = \frac{E_k}{E_{sys}} \times 100\% \tag{13}$$

The energy efficiency of the improved system can be expressed as follows:

$$\eta_2 = \frac{E_k}{E_{sec}} = \frac{E_k}{E_{sys} - E_{rec}} \times 100\% \tag{14}$$

The calculation method for each energy value is as follows:

$$E_{sys} = \frac{1}{2} C_1 U_0^2 \tag{15}$$

$$E_{rec} = \frac{1}{2} C_1 U_1^2 + \frac{1}{2} C_2 U_2^2 \tag{16}$$

$$E_{\text{loss}} = E_{sys} - E_k - E_{rec} \tag{17}$$

where U_1 is the voltage of capacitor C_1 and U_2 is the voltage of capacitor C_2 after the end of the third discharge stage

$$E_k = \int_a^b \int_0^d F(x, y)\text{dxdy} \tag{18}$$

where d is the maximum displacement of each segment of the line element, a and b are the left and right ends of the cross-section of the welding zone respectively, and F is the electromagnetic force.

4 Establishment of a simulation model

Magnetic pulse welding is a very complicated physical process. Much data on the energy utilization rate of the calculation system are difficult to be obtained by artificial calculation or experiment, so it is necessary to establish a numerical model for this process. Each part of the numerical model established in this paper is made of a 1060 aluminum flyer plate, T2 copper base plate and chrome-zirconium copper (CuCrZr) driving coil. Because the coupling between multiple physical fields is involved, the two-dimensional model of magnetic pulse welding is established by using COMSOL Multiphysics finite element software. The model uses three modules: circuit, magnetic field, and solid mechanics.

4.1 Circuit module

This module is used for circuit analysis. The impulse current is solved by Kirchhoff's current law and Kirchhoff's voltage law. The current data solved by the circuit module will be transferred to the magnetic field module as input through the discharge coil for the calculation of electromagnetic force. In this model, the current data used by the circuit module is simulated by Simulink. The circuit parameters in the simulation process are shown in Table 1.

4.2 Magnetic field module

The module is used for magnetic field analysis of welding equipment. Firstly, the spatial distribution of the magnetic field is solved by Maxwell's equation, and then the electromagnetic force acting on the flyer plate is calculated and transferred to the solid mechanic's module as an input load. In this module, the induced eddy current in the coil, channel, and flyer plate can be described by the following equation:

$$\nabla \times \mathbf{E} = -\frac{\partial \mathbf{B}}{\partial t} + \nabla \times (\mathbf{v} \times \mathbf{B}) \tag{19}$$

$$J = \gamma \mathbf{E} \tag{20}$$

Table 1 Circuit parameters

Parameters	Value
Discharge capacitance C_1/μF	148.5
Auxiliary capacitance C_2/μF	80
Resistance of main discharge circuit R_1/mΩ	3.9
Auxiliary circuit resistance R_2/mΩ	0.2
The inductance of the main discharge circuit L/nH	319
C_1 initial voltage/kV	9

where E is the electric field intensity, B is the magnetic flux density, v is the deformation speed of the flyer plate, J is the induced current density, and γ is the conductivity of metal materials. The electromagnetic parameters in the simulation are shown in Table 2.

4.3 Solid mechanics module

The module is mainly used for stress analysis of discharge coil and plastic deformation motion of flyer plate. The output will be fed back to the magnetic field module to realize the coupling calculation between the magnetic field and the structure. Table 3 shows the detailed mechanical parameters of the materials used in the simulation. The flyer plate will undergo plastic deformation motion under the action of the electromagnetic force, and its motion satisfies the following equation:

$$\nabla \cdot \sigma + \mathbf{F}_v = \rho \frac{\partial^2 \mathbf{u}}{\partial t^2} \tag{21}$$

σ is the stress tensor of the flyer plate, F_v is the volume density vector of the electromagnetic force, ρ is the density of the flyer plate, and u is the displacement vector.

The coupling mode of the three physical field modules is shown in Fig. 6.

5 Results and discussion

5.1 Choice of capacitance C_2 capacity

In this magnetic pulse welding system, most of the energy loss is Joule heat; so to improve the system energy utilization, Joule heat should be reduced as much as possible. The values of resistance, inductance, and capacitor C_1 are fixed throughout the circuit, so the value of capacitor C_2 should be adjusted to reduce the Joule heat. Joule heat can be calculated by the following formula:

$$W = R \int_0^t i^2(\tau) d\tau \tag{22}$$

In this MPW system, there are two circuits, the main discharge circuit and the auxiliary circuit. Through simulation, the current waveforms of two loops can be obtained, and the capacitance value of capacitor C_2 can be changed to obtain a series of current waveforms, as shown in Fig. 7.

As can be seen from Fig. 7, with the increase of capacitance C_2, the peak current of the main discharge loop remains unchanged, but the duration of the second discharge stage gradually increases. The peak current of the auxiliary loop and the total duration of the second discharge stage and the third discharge stage is increasing gradually. As can be seen from Eq. (21), with the increase of capacitance C_2, the Joule heat generated by the whole system also increases, and the changing trend is shown in Fig. 8.

Therefore, the smaller the capacity of capacitor C_2, the smaller the system energy loss. However, as the capacity of capacitor C_2 decreases, the voltage that C_2 finally bears will also increase, as shown in Fig. 9.

Because the higher the capacitor rated voltage, the higher the capacitor cost, taking into account the above factors, this paper finally determined the capacity value of C_2 as 80 μF.

Table 2 Electromagnetic parameters of each material

Materials	Conductivity (S/m)	Relative permeability
1060 Al	3.53×10^7	1
CuCrZr	4.52×10^7	1
T2 Cu	5.71×10^7	1

Table 3 Mechanical parameters of each material

Materials	Young's modulus/GPa	Poisson's ratio	Initial yield stress/MPa
1060 Al	80.7	0.34	35
CuCrZr	117	0.34	495
T2 Cu	135	0.34	110

5.2 Experimental analysis

In order to verify the feasibility of the improved MPW circuit proposed in this paper, we carry out an experimental analysis. In the experiment, the current waveforms of the main discharge circuit of the MPW system before and after improvement were captured, respectively, and compared

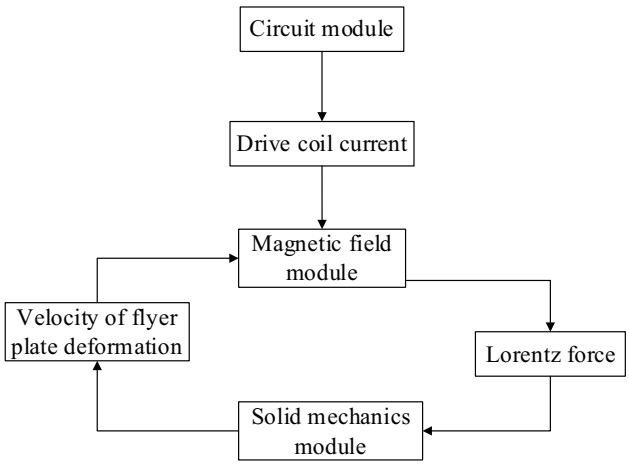

Fig. 6 Coupling mode of multiple physical fields

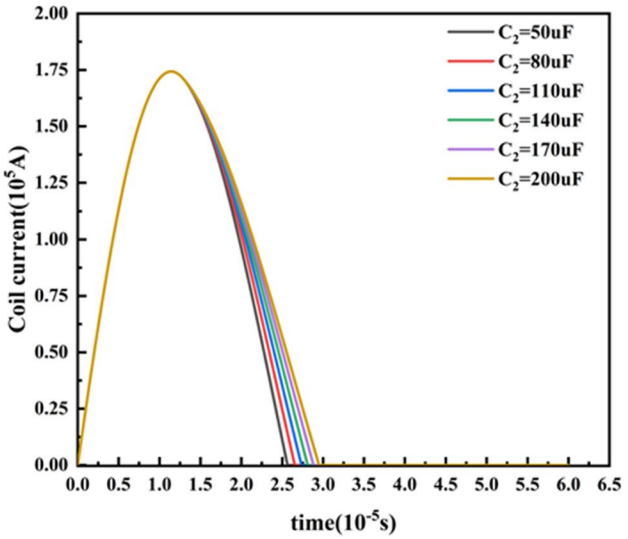

(a) main discharge circuit current waveform

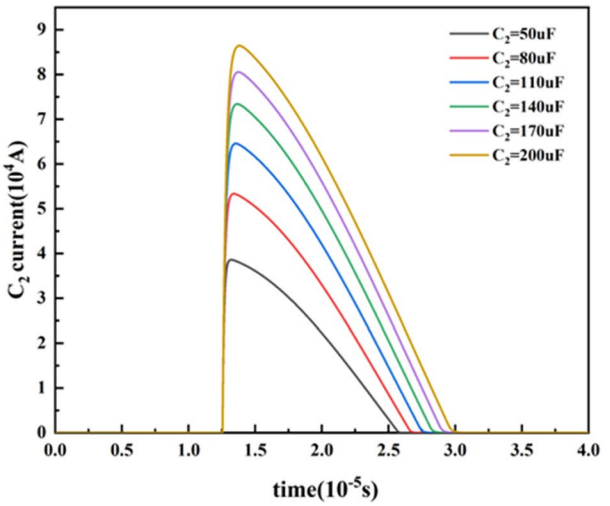

(b) Auxiliary loop current waveform

Fig. 7 Current waveform of each loop with capacitance C_2 changed

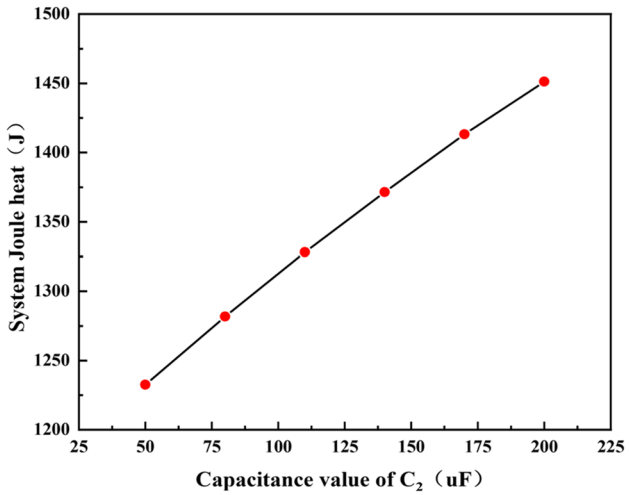

Fig. 8 Trend of Joule heat

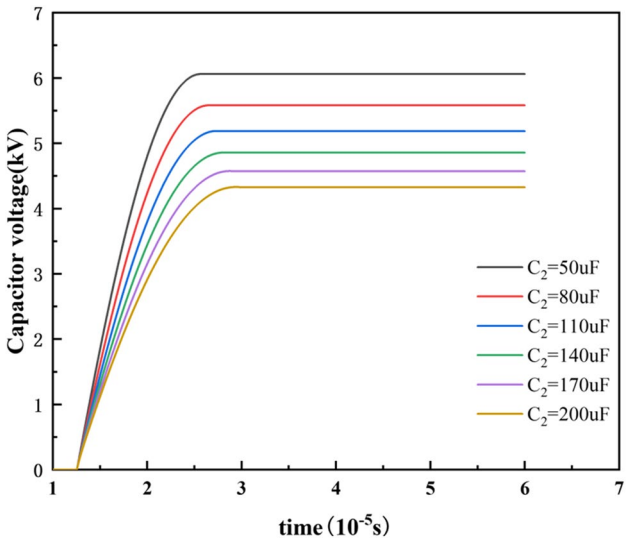

Fig. 9 Voltage variation trend of capacitor C_2

with the current waveforms of the main discharge circuit obtained by simulation, as shown in Fig. 10. The waveform of the actual main discharge circuit before and after the improvement is roughly consistent with that of the simulated main discharge circuit. It is verified that the improved MPW circuit can realize that the current of the main discharge circuit can rapidly decay to near 0 after the first positive half cycle, so as to achieve the purpose of improving the energy efficiency of the MPW system.

5.3 Simulated analysis

Based on the initial circuit parameters of the past work and the selected capacitor C_2, the Simulink circuit simulation model and COMSOL Multiphysics simulation model are built. The main function of the Simulink simulation model is to take the data in the main discharge circuit as the input of the circuit module of the COMSOL Multiphysics model and calculate the energy E_{rec} recovered by the system through formula (16). COMSOL Multiphysics model is used to verify the feasibility of this method, that is, whether effective welding can be formed. The criterion is the Al-Cu welding window theory. In addition, the COMSOL Multiphysics model can also calculate the work E_k done by the electromagnetic force on the flyer plate through Eq. (17).

The simulation results show that the pulse current of the main discharge loop reaches its peak value at 12.55 μs after the discharge capacitor starts, and the peak current is 157.3 kA. When the main discharge circuit current reaches

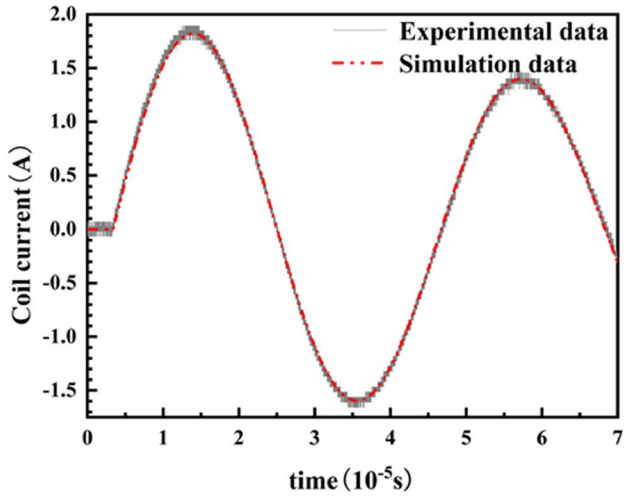

(a) Main discharge circuit current before improvement

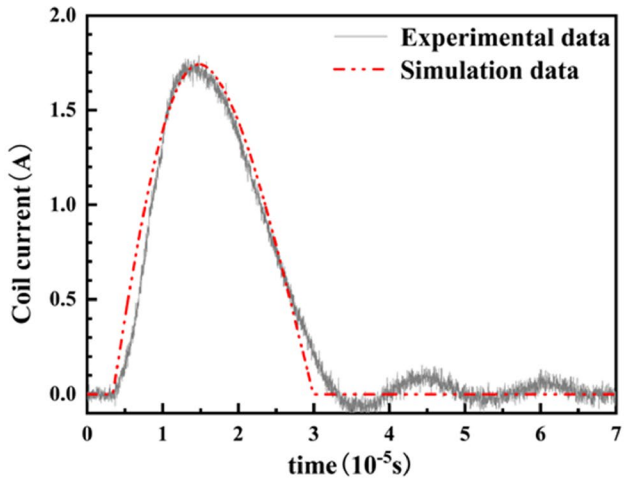

(b) Main discharge circuit current after improvement

Fig. 10 Comparison between experimental current waveform and simulation current waveform

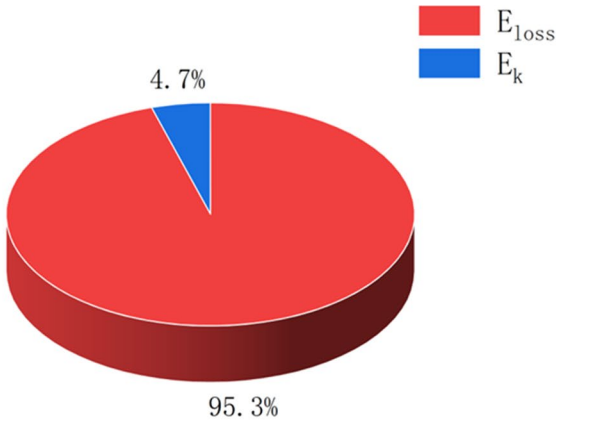

(a) Energy distribution before improvement

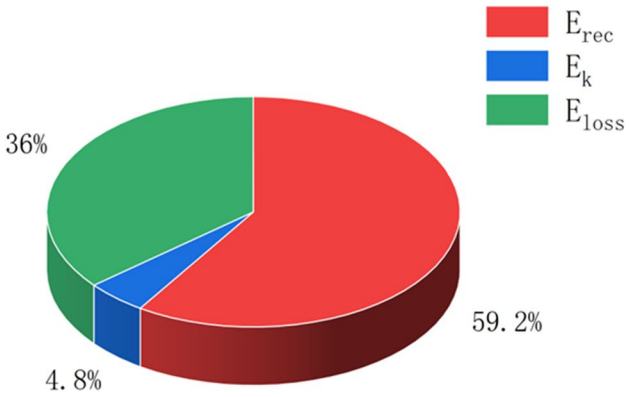

(b) Energy distribution after improvement

Fig. 11 Energy distribution of simulation system before and after circuit improvement

the peak, the circuit will enter the second discharge stage from the first discharge stage. The duration of the second discharge stage was 13.97 μs. When the system changes from a transient state to a steady state, the voltage of C_1 and C_2 is 5582.5 V. According to the calculation method of Eqs. (15) ~ (18), the energy distribution of the simulation system before and after circuit improvement can be obtained, as shown in Fig. 11.

According to the calculation method of Eqs. (13)–(14), the energy utilization rate of the system before and after improvement is 5.1% and 13.33%, respectively, and the energy utilization rate is increased by 261.5%. Energy loss decreased from 95.3 to 36% after improvement.

According to the welding window theory, the moving velocity Vc of the collision front point (CFP) and the collision angle β are respectively the horizontal axes and the vertical axis to form a rectangular coordinate system. When the welding process (V_C, β) falls in the rectangular coordinate system under a specific area, effective welding can be formed, and the area calls the welding window [17]. The collision front point and collision angle are shown in Fig. 12. The value range of the welding window is related to the material and geometric parameters of the plate. For different materials and plate thicknesses, the corresponding welding window is also different [18]. In this model, the thickness of the Cu plate and Al plate is 1 mm, and the materials are T2 Cu and 1060 Al. The lower limit of the welding window can be expressed by Eq. (23) [19].

$$\beta = \sqrt{\frac{2.45 \times 10^8}{2700 \cdot V_c^2}} \tag{23}$$

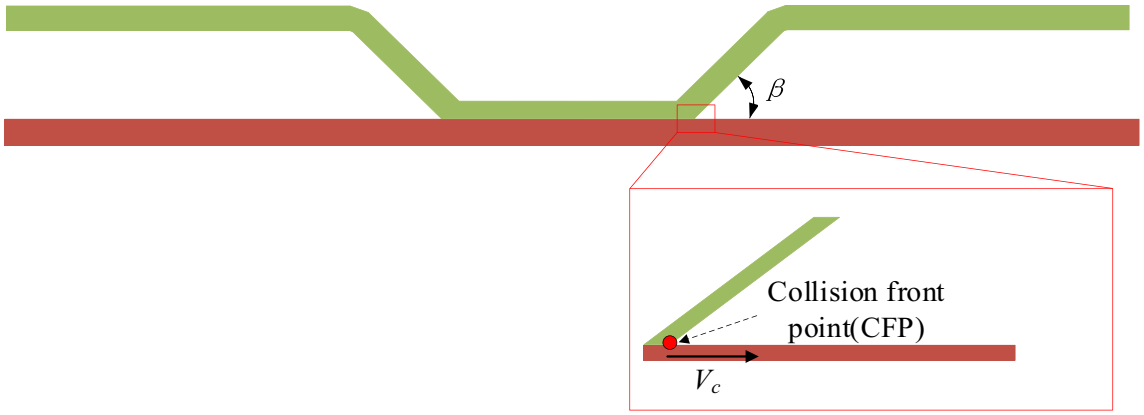

Fig. 12 Schematic diagram of collision front point (CFP) and collision angle β

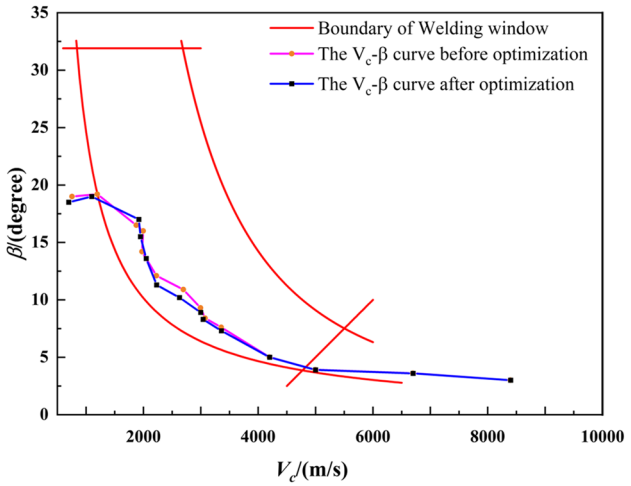

Fig. 13 Welding window and simulation data

The upper limit of the welding window was obtained by extracting the upper limit curve data of MPW of the Cu-Al plate based on Vc and β [19]. The maximum impact angle is 31.9° [20]. Finally, data points (V_C, β) of 14-time points in a simulation were selected and compared with those before improvement. The welding window and simulation results are shown in Fig. 13.

As shown in Fig. 11, Vc-β curves before and after improvement are basically consistent and located in the welding window, so the improved circuit with this method does not affect the final welding effect.

6 Conclusion

In this paper, the low energy utilization rate of traditional MPW circuits is introduced in detail, and a magnetic pulse welding energy efficiency improvement method based on auxiliary capacitance is proposed. The effect of auxiliary capacitance on energy loss and the improved energy distribution are studied by simulation. The efficiency of the optimized system is improved significantly. Therefore, the following conclusions are drawn:

1. The larger the capacity of the auxiliary capacitor, the more Joule heat is generated by the system, but the smaller the capacity of the auxiliary capacitor, the higher the voltage it will withstand. In order to improve the energy utilization rate of the system and ensure the stable operation of the circuit, the capacity of the auxiliary capacitor is set at 80 μF.
2. Through experimental analysis, the improved circuit can realize that the current of the main discharge circuit can rapidly decay to near 0 after the first positive half cycle, so as to achieve the purpose of improving the energy efficiency of MPW system.
3. Through simulation analysis, the energy loss of the improved circuit is reduced from 95.3 to 36%, and the energy utilization rate is increased by 261.5%. Greatly improved the system energy utilization rate.
4. According to the welding window theory, the welding quality of this method is analyzed. The results show that this method can improve the energy utilization rate of the system under the premise of guaranteeing the welding quality, and providing technical support for the industrialization of magnetic pulse welding

Author contribution All authors contributed to the study conception and design. Material preparation, data collection, and analysis were performed by Wentao Liu, Wenxiong Peng, Zhi Li, and Huaiqing Zhang. The first draft of the manuscript was written by Wentao Liu, and all authors commented on previous versions of the manuscript. All authors read and approved the final manuscript.

Funding This work was supported by the National Natural Science Foundation of China (Grant numbers 51877014).

Declarations

Competing interests The authors declare no competing interests.

References

1. Taban E, Gould JE, Lippold JC (2010) Characterization of 6061–T6 aluminum alloy to AISI 1018 steel interfaces during joining and thermo-mechanical conditioning. Mater Sci Eng A 527:1704–1708. https://doi.org/10.1016/j.msea.2009.10.059
2. Torkamany MJ, Tahamtan S, Sabbaghzadeh J (2010) Dissimilar welding of carbon steel to 5754 aluminum alloy by Nd:YAG pulsed laser. Mater Des 31:458–465. https://doi.org/10.1016/j.matdes.2009.05.046
3. Yan YB, Zhang ZW, Shen W, Wang JH, Zhang LK, Chin BA (2010) Microstructure and properties of magnesium AZ31B–aluminum 7075 explosively welded composite plate. Mater Sci Eng A 527:2241–2245. https://doi.org/10.1016/j.msea.2009.12.007
4. Fuller CB, Mahoney MW, Calabrese M, Micona L (2010) Evolution of microstructure and mechanical properties in naturally aged 7050 and 7075 Al friction stir welds. Mater Sci Eng A 527:2233–2240. https://doi.org/10.1016/j.msea.2009.11.057
5. Atasoy E, Kahraman N (2008) Diffusion bonding of commercially pure titanium to low carbon steel using a silver interlayer. Mater Charact 59:1481–1490. https://doi.org/10.1016/j.matchar.2008.01.015
6. Liu J, Watanabe I, Yoshida K, Atsuta M (2002) Joint strength of laser-welded titanium. Dent Mater 18:143–148. https://doi.org/10.1016/S0109-5641(01)00033-1
7. DebRoy T, David SA (1995) Physical processes in fusion welding. Rev Mod Phys 67:85–112. https://doi.org/10.1103/RevModPhys.67.85
8. Kang B-Y (2015) Review of magnetic pulse welding. J Weld Join 33:7–13. https://doi.org/10.5781/JWJ.2015.33.1.7
9. Wang H, Wang Y (2019) High-velocity impact welding process: a review. Metals 9:144. https://doi.org/10.3390/met9020144
10. Li Z, Peng W, Chen Y, Liu W, Zhang H (2023) Analysis of energy transfer process in magnetic pulse welding and optimization of system efficiency. Int J Adv Manuf Technol 125:2425–2434. https://doi.org/10.1007/s00170-023-10905-4
11. Khalil C, Marya S, Racineux G (2020) Magnetic pulse welding and spot welding with improved coil efficiency—application for dissimilar welding of automotive metal alloys. J Manuf Mater Process 4:69. https://doi.org/10.3390/jmmp4030069
12. Zhang H, Yang Z, Ren L (2019) Experimental investigation on structure parameters of E-shaped coil in magnetic pulse welding. Mater Manuf Processes 34:1701–1709. https://doi.org/10.1080/10426914.2019.1689263
13. Deng F, Cao Q, Han X, Li L (2018) Electromagnetic pulse spot welding of aluminum to stainless steel sheets with a field shaper. Int J Adv Manuf Technol 98:1903–1911. https://doi.org/10.1007/s00170-018-2208-2
14. Li C, Zhou Y, Wang X, Shi X, Liao Z, Du J, Yao C (2020) Influence of discharge current frequency on electromagnetic pulse welding. J Manuf Process 57:509–518. https://doi.org/10.1016/j.jmapro.2020.06.038
15. Li Z, Peng W, Chen Y, Liu W, Zhang H (2022) Simulation and experimental analysis of Al/Ti plate magnetic pulse welding based on multi-seams coil. J Manuf Process 83:290–299. https://doi.org/10.1016/j.jmapro.2022.09.015
16. Zhou Y, Li C, Shi X, Wang P, Shen T, Mi Y, Ma Y (2022) Evaluation model of electromagnetic pulse welding effect based on Vc-β trajectory curve. J Market Res 20:616–626. https://doi.org/10.1016/j.jmrt.2022.07.069
17. Carpenter SH, Wittman RH (1975) Explosion welding. Annu Rev Mater Sci 5:177–199. https://doi.org/10.1146/annurev.ms.05.080175.001141
18. Groche P, Becker M, Pabst C (2017) Process window acquisition for impact welding processes. Mater Des 118:286–293. https://doi.org/10.1016/j.matdes.2017.01.013
19. HoseiniAthar MM, Tolaminejad B (2015) Weldability window and the effect of interface morphology on the properties of Al/Cu/Al laminated composites fabricated by explosive welding. Mater Des 86:516–525. https://doi.org/10.1016/j.matdes.2015.07.114
20. AkbariMousavi SAA, Al-Hassani STS (2008) Finite element simulation of explosively-driven plate impact with application to explosive welding. Mater Des 29:1–19. https://doi.org/10.1016/j.matdes.2006.12.012